Materials Science and Engineering B 124–125 (2005) 444–448

www.elsevier.com/locate/mseb

The effect of ion implantation energy and dosage on the microstructure of the ion beam synthesized $FeSi_2$ in Si

Y.T. Chong [a,c], Q. Li [a,c,*], C.F. Chow [b,c], N. Ke [b,c], W.Y. Cheung [b,c], S.P. Wong [b,c], K.P. Homewood [d]

[a] *Department of Physics, The Chinese University of Hong Kong, Hong Kong, China*
[b] *Department of Electronic Engineering, The Chinese University of Hong Kong, Hong Kong, China*
[c] *Materials Science and Technology Research Centre, The Chinese University of Hong Kong, Hong Kong, China*
[d] *School of Electronics Engineering, Computer and Mathematics, University of Surrey, Guildford, Surrey GU2 7XH, UK*

Abstract

Nanometer-sized β-$FeSi_2$ precipitates are formed in Si by ion beam synthesis (IBS). A systematic study is carried out to investigate the correlation among the implantation parameters, the microstructure, and the luminescence properties. On the one hand, we found additional orientation relationships (ORs) appear between the β-$FeSi_2$ and the Si with improved lattice coherence between the two, when the ion implantation energy is increased. On the other hand, the degree of preferential orientation deteriorates and leads to poor lattice coherence between the particles and Si matrix when the iron ion is overdosed. These microstructure changes lead to different luminescence properties (intensity, peak position and shape) of the β-$FeSi_2$ particles accordingly.

Keywords: Ion implantation energy; Semiconducting β-$FeSi_2$; Ion beam synthesis

1. Introduction

Semiconducting β-$FeSi_2$ has orthorhombic structure with lattice constants of $a = 0.9863$ nm, $b = 0.7791$ nm, $c = 0.7833$ nm [1]. The band gap of the material is reported to be ∼0.8 eV (corresponds to a wavelength of 1.55 μm), matching the preferred wavelength window for optical communication systems [2–3]. Together with its promising optical properties, the convenience of incorporating $FeSi_2$ into the current Si-based microelectronics for photonic applications has attracted great research attention in the past decade. Various techniques have been employed to prepare β-$FeSi_2$, such as pulsed laser deposition (PLD) [4], reactive deposition epitaxy (RDE) [5], molecular beam epitaxy (MBE) [6], and ion beam assisted deposition (IBAD) [7]. Among them, ion beam synthesis (IBS) is one of the most widely used techniques and is capable of producing samples with $FeSi_2$-particle/Si-matrix configuration, in which the β-$FeSi_2$ phase serves as effective light emitting materials [8–10].

Various processing parameters of IBS play important roles in determining the microstructure of $FeSi_2$ such as phase, lattice coherence with the Si matrix, and strain, etc. which further affect its luminescence properties. In fact, several orientation relations between the $FeSi_2$ and the Si have been identified experimentally, and the correlations between the specific microstructure and luminescence properties of the material have been elaborated. For example, Maeda et al. showed that better interfacial structure between the β-$FeSi_2$ precipitates and the Si would enhance the photoluminescence (PL) intensity [11], Spinella and co-workers showed that the large unstrained β-$FeSi_2$ precipitates give the PL signal at 1.54 μm [10]. On the other hand, it has also been theoretically predicted that the presence of suitable strain changes the β-$FeSi_2$ band gap value as well as its nature from indirect to direct [12–13]. Unfortunately, the available literature results are both limited and scattered. In many cases, discrepancies exist among individual works. Therefore, a systematic study to investigate the correlation among the implantation parameters, the microstructure and the luminescence properties is needed, in order to understand the fundamental physics that govern the luminescence properties of the $FeSi_2$, which would further guide the engineering process of this promising photonic material.

In this work, $FeSi_2$ precipitates are formed in Si using IBS with two series of systematically designed processing parameters. The microstructures of the resulted $FeSi_2$ precipitates were

* Corresponding author. Tel.: +852 2609 6323; fax: +852 2603 5204.
E-mail address: liquan@phy.cuhk.edu.hk (Q. Li).

0921-5107/$ – see front matter © 2005 Elsevier B.V. All rights reserved.
doi:10.1016/j.mseb.2005.08.042

investigated using transmission electron microscopy (TEM), and the corresponding photoluminescence properties were examined. The effect of ion implantation energy and dosage on the microstructure evolution and the luminescence properties of the β-$FeSi_2$ particles are discussed.

2. Experimental

The samples were prepared using iron ion implantation into (1 0 0) p-Si wafer (resistivity ∼15–25 Ωcm) using a metal vapor vacuum arc (MEVVA) ion source. In order to investigate the effects of both the implantation energy and the ion dosage on the microstructure and the luminescence properties of the samples independently, we designed two experiment series. In the implantation energy series, the three samples, which are referred to EN1, EN2, and EN3, were implanted at extraction voltages of 40 kV, 60 kV, and 80 kV, respectively, at a fixed total dose of 5×10^{15} ions/cm^2. In the dosage series, the extraction voltage was kept fixed at 80 kV with three different doses of 1×10^{15}, 5×10^{15} and 1×10^{16} ions/cm^2, for the samples DO1, DO2, and DO3, respectively. The implantation temperature was maintained at approximately −100 °C for all the samples so that a dislocation-free layer would be expected after annealing according to a previous report on the study of implantation temperature effect [14]. The as-implanted samples were then subjected to a dual step annealing process, i.e. firstly annealed using a rapid thermal annealing (RTA) at 850 °C for 20 s, followed by a furnace annealing (FA) at 850 °C for 10 h. The microstructure characterizations of the annealed samples were carried out using transmission electron microscopy (Philips CM120, and Tecnai 20 ST). The detailed phase identification and orientation relation between the Fe–Si phase and the Si matrix were examined using transmission electron diffraction (TED). The luminescence properties of the annealed samples were studied by photoluminescence (PL), which were performed at 80 K using the 514 nm line of an argon laser with a power of 150 mW as the excitation source. The light emission was dispersed using a1 m monochromator and detected by a liquid nitrogen cooled Ge detector.

3. Results

The TEM results of the as-implanted samples (not shown here) revealed that an amorphous layer of Fe–Si mixtures was formed on top of the crystalline Si. The thickness of the layer is determined by the implantation parameters such as ion energy and ion dosage. The iron silicide phase would precipitate out only after the annealing process.

3.1. Ion energy series

$FeSi_2$ particles of similar sizes are formed in sample EN1, EN2, and EN3 after annealing. The selected area electron diffraction patterns (SADP) taken from their planview TEM samples are shown in Fig. 1(a)–(c), respectively. The SADPs were taken with the electron beam parallel to the Si [1 0 0] zone axis. Extra diffraction spots not belonging to Si are observed (as marked by arrows). In order to identify the phase origin of these extra diffraction spots, micro-diffractions (μ-diffraction) are taken from the particles that give the specific diffractions as marked by arrow d–f in Fig. 1(a)–(c), respectively. All of the μ-diffractions (Fig. 1(d)–(f)) can be indexed to the orthorhombic β-$FeSi_2$ phase (S.G: Cmca (64)) [1,15] but having different orientation relationships (OR) with the Si matrix.

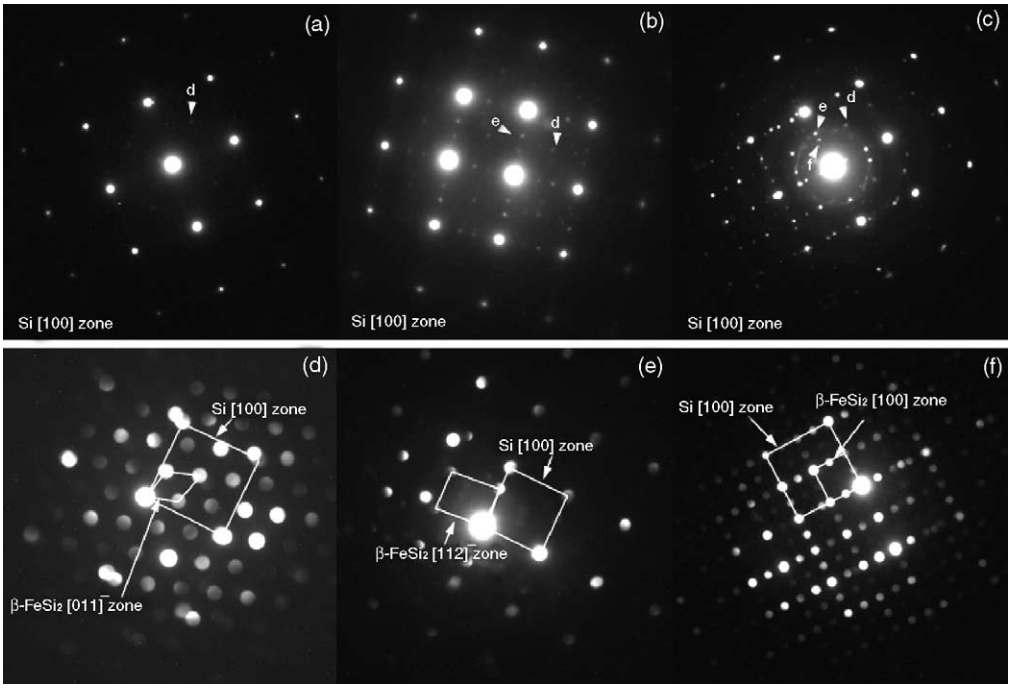

Fig. 1. (a)–(c) are the SADPs taken from planview EN1, EN2 and EN3 respectively; (d)–(f) are the μ-diffraction patterns taken from the particles corresponding to the specific diffraction spots as marked by arrows d–f in (a)–(c), respectively.

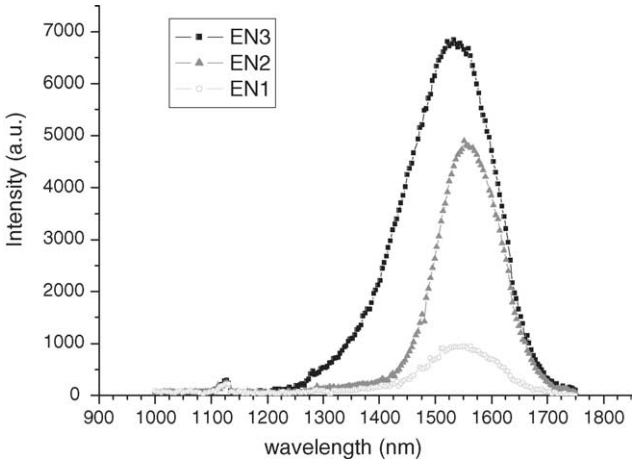

Fig. 2. PL spectra of EN1, EN2 and EN3.

Single OR (I) is observed in sample EN1 (Fig. 1(d)), with $[0\,1\,\bar{1}]_{\beta\sim}//[1\,0\,0]_{Si}$, $(0\,2\,2)_{\beta\sim}//(0\,0\,4)_{Si}$ and $(2\,0\,0)_{\beta\sim}//(0\,4\,0)_{Si}$. Besides the OR observed in EN1, one more OR (II) is observed in EN2 (Fig. 1(e)), with $[1\,1\,\bar{2}]_{\beta\sim}//[1\,0\,0]_{Si}$ and $(\bar{2}\,2\,0)_{\beta\sim}//(0\,2\,2)_{Si}$. Other than the ORs demonstrated in Fig 1(d) and (e), still another one (OR (III)) is observed in sample EN3 (Fig. 1(f)), with $[1\,0\,0]_{\beta}//[1\,0\,0]_{Si}$, $(0\,2\,0)_{\beta}//(0\,2\,2)_{Si}$, and $(0\,0\,1)_{\beta}//(0\,2\,2)_{Si}$. By comparing the measured *d*-spacing in the diffraction pattern and the calculated ones from the standard lattice spacing of β-$FeSi_2$, one can obtain the strain values corresponding to the specific ORs. The only OR (I) observed in EN1 has strain of 0.56% along the $[1\,0\,0]_{\beta}$ direction, and 1.81% along the $[0\,1\,1]_{\beta}$ direction. The additional OR (II) identified in EN2 corresponds to strain of −1.53% and −2.89% in the $[5\,8\,0]_{\beta}$ and the $[5\,8\,8]_{\beta}$ crystalline directions, respectively. Similarly, the strain values in the second additional OR (III) observed in EN3 were determined to be −1.63% along the $[0\,1\,0]_{\beta}$ direction and −2.16% along the $[0\,0\,1]_{\beta}$ direction.

The PL spectra taken from the ion energy series samples are shown in Fig. 2. All of them give broad peaks at ∼1550 nm. EN1 gives the lowest emission intensity, which is much improved in sample EN2. Both samples have emission peaks centered at ∼1550 nm. Sample EN3 demonstrates the strongest emission among the three, but with a blue-shifted peak position at a shorter wavelength (∼1530 nm).

3.2. Ion dosage series

Fig. 3(a)–(c) are the planview TEM images of the annealed samples DO1, DO2, and DO3, respectively. These images show that dark spherical particles were formed after the dual step annealing. The number of particles is significantly fewer in DO1 than in DO2 and DO3. The particle size of DO1 (10–30 nm in diameter) is smaller than those in DO2 and DO3 (10–50 nm in diameter). In order to identify the phase of the particles, SADPs were taken with electron beam parallel to the Si [1 0 0] zone axis, as shown in Fig. 3(d)–(f). Only one set of diffraction spots, originating from the Si lattice is clearly observed in DO1 (Fig. 3(d)), indicating the small amount of Fe–Si phase in the sample. Extra diffraction spots that do not belong to Si are observed in DO2 (the same sample as EN3) (Fig. 3(e)), which results have been described in the previous paragraph (Fig. 1(c)). As a comparison, polycrystalline ring patterns that can be indexed to the β-$FeSi_2$ phase are observed in DO3 (Fig. 3(f)), suggesting that no preferential OR occurs between the β-$FeSi_2$ and the Si matrix. Strain also exists in the $FeSi_2$ particles in DO3, with a value of −1.63%

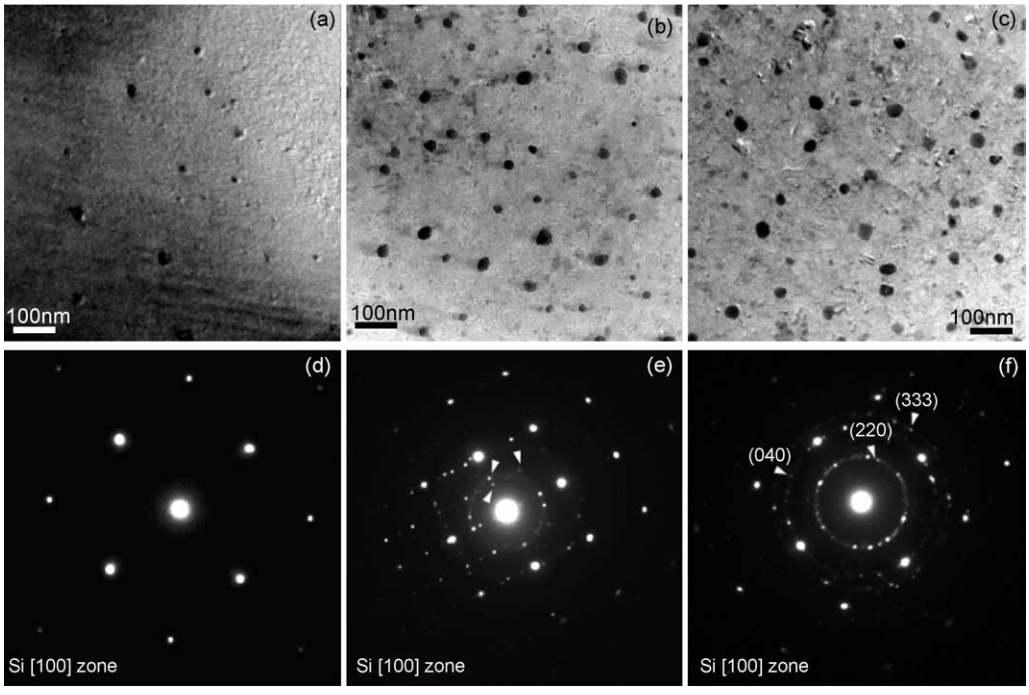

Fig. 3. (a)–(c) are the planview TEM images taken from DO1, DO2, and DO3, respectively; (d)–(f) are the corresponding SADPs of the three samples following the same order.

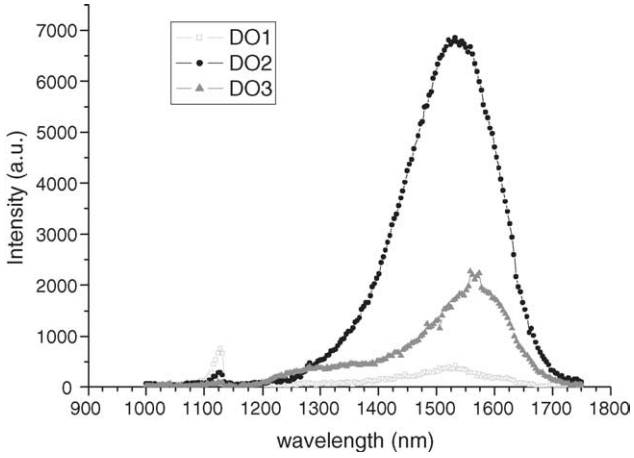

Fig. 4. PL spectra of DO1, DO2 and DO3.

along the $[0\,1\,0]_\beta$ direction, 3.42% along the $[5\,8\,0]_\beta$ direction and 2.23% along the $[5\,8\,8]_\beta$ direction.

The PL spectra taken from the ion dosage series samples are shown in Fig. 4. While the lowest dose sample DO1 gives the weakest emission intensity, the intermediate dose sample DO2 gives the strongest emission intensity with a broad peak centered at ~1530 nm. The emission intensity of the largest dose sample DO3 however lies in-between those of DO1 and DO2 and gives a broad peak with the center position red-shifted to ~1560 nm. In addition, there are two small spikes situated at 1550 and 1570 nm on top of the broad peak and an extra shoulder ranging from 1200 to 1400 nm.

4. Discussions

4.1. Ion energy series

In the ion energy series, it is observed that additional ORs between the β-$FeSi_2$ and the Si appear when the ion implantation energy increases (Fig. 1). The only OR (I) observed in EN1 associates with the worst lattice coherence in-between the β-$FeSi_2$ particles and the Si substrate, as none of their crystalline directions (planes) are perfectly aligned. Slightly improved lattice coherence is obtained in the OR (II) at the expense of larger strains in the β-$FeSi_2$ phase. Finally, the best lattice coherence is achieved in the OR (III), as suggested by the strain analysis of OR (III). The exact physics of how the increased ion implantation energy promotes the lattice coherence between the β-$FeSi_2$ and the Si is not clearly understood. Nevertheless, we speculate that it is related to the increased strain energy needed to achieve better lattice coherence, which can be provided by the increased ion implantation energy. This is consistent with the experimental observation that such improved lattice coherence associates with larger strain of the $FeSi_2$ phase.

The broad PL peaks observed in EN1, EN2 and EN3 may originate from both the β-$FeSi_2$ [16] and the Si dislocation (D1) related emissions [17]. Nevertheless, the facts that the line shape of the D1 emission is very narrow, and we have not observed any obvious dislocations in the TEM analysis suggest that Si dislocation (D1) related emission is not likely. The absence of dislocation formation and hence the D1 emission in these samples is due to the low implantation temperature used in accordance with a previous study on the implantation temperature effect [14]. Subtle difference exists in the exact PL peak positions of the three samples. This may be attributed to the existence of $FeSi_2$ phases at different strain states in the three samples [12–13].

The PL intensity is observed to increase from sample EN1 to EN3 as the ion implantation energy increases (Fig. 2). In general, the PL intensity would be affected by several factors: (1) The amount of the light emitting phase; (2) the existence of non-radiative recombination centers; and (3) the nature of the material band gap. Firstly, we found that the amount of β-$FeSi_2$ is much less in EN1 than those in EN2 and EN3, as suggested by the diffraction intensity of the $FeSi_2$ phase in the three samples (Fig. 1a–c). This would contribute to the observed weak PL emission in EN1 than those in EN2 and EN3. Secondly, the orientation analysis of the β-$FeSi_2$ phase and the Si matrix suggests that EN1 suffers from the worst lattice coherence between the two, which becomes better in EN2, and further improves in EN3. Worse lattice coherence suggests more dangling bonds at the $FeSi_2$/Si interface, which usually serve as non-radiative recombination centers and lead to loss of the luminescence intensity. Thirdly, the different strain states associated with the three ORs may lead to changes in the band gap nature of the material, i.e. direct–indirect band gap transition. In fact, Abram et al. have predicted in their theoretical calculation of the β-$FeSi_2$ electronic structure that although the relaxed β-$FeSi_2$ is an indirect band gap semiconductor, compressive strains along $[0\,1\,0]_\beta$ (−1.4%) and $[0\,0\,1]_\beta$ (−1.8%) would change its band gap from indirect to direct [12]. These calculated strain values are close to our experimental strain values associated with OR (III) observed in the sample EN3. Obviously, the direct band gap material is a much more efficient light emitter compared to the indirect band gap one. This may also count for the highest PL intensity observed in EN3.

4.2. Ion dosage series

It is impossible to analyze the OR between the $FeSi_2$ particles and the Si in DO1 due to the limited amount of the $FeSi_2$ phase in the sample, as can be seen from both the low magnification TEM image (Fig. 3a) and the corresponding SADP (Fig. 3d). Three specific ORs are identified in DO2 (the same sample as EN3), of which the lattice coherence in-between the β-$FeSi_2$ and the Si has been discussed in the previous paragraph. The fact that random ORs between the $FeSi_2$ and the Si exist in DO3 suggests the deteriorated lattice coherence in-between the two. It is reasonable that the degree of preferential orientation degrades when the ion dosage increases to a certain extent, as the resulted severe damage of the Si matrix would be no longer capable of accommodating the $FeSi_2$ particles with specific ORs.

The extremely weak PL signal of DO1, which results from the insufficient light-emitting phase ($FeSi_2$) in the sample, makes it difficult to locate the accurate peak position. The main broad peak observed in the PL spectra of both DO2 and DO3 originates from the β-$FeSi_2$ phase. The difference in the peak position of

the two samples is most likely caused by the different strain states of the $FeSi_2$ phase, as discussed earlier. One should note that two additional features are observed in DO3 other than the main peak. One of them is the two small spikes superimposed on the main broad peak, which can be attributed to the Si dislocation (D1) related emissions, based on their line shapes and positions [9,17]. The other feature, i.e. the broad shoulder ranging from 1200 to 1400 nm may be ascribed to the emissions originating from some implantation induced defects in the sample, which cannot be recovered during the annealing process due to the high dose in DO3.

Although DO3 contains more β-$FeSi_2$ particles, its PL intensity is lower than that of DO2. This can be understood when considering the bad lattice coherence in-between the β-$FeSi_2$ and the Si, and thus the large number of dangling bonds forming at the $FeSi_2$/Si interface in DO3, which act as non-radiative recombination centers and reduce the light emission efficiency.

5. Conclusions

Nanometer-sized β-$FeSi_2$ particles are formed in Si using Fe ion implantation followed by dual step annealing. The two independent implantation parameters (ion implantation energy and dosage) play important roles in affecting the microstructure and thus the PL properties of the β-$FeSi_2$ particles. Additional ORs between the $FeSi_2$ and the Si are observed when the ion implantation energy is increased, resulting in improved lattice coherence between the particles and the Si matrix and different strain states of the $FeSi_2$ phase. These microstructure changes agree well with the PL characteristics of the samples, including the increase of PL intensity with the OR improvements and the difference in the PL peak positions. On the other hand, the degree of the preferential orientation deteriorates leading to poorer lattice coherence between the particles and the Si matrix, as the result of the Fe ion overdose. This corresponds well with the PL intensity decrease in the overdosed sample.

Acknowledgements

This work is partially supported by the Research Grants Council of Hong Kong SAR (ref. number: CUHK4231/03E and an RGC direct grant in the Chinese University of Hong Kong, under Project no. 2060261.

References

[1] JCPDF data file, International Center for Diffraction Data (ICDD), 74-1285.
[2] D. Leong, M. Harry, K.J. Reeson, K.P. Homewood, Nature 387 (1997) 686.
[3] M.C. Bost, J.E. Mahan, J. Appl. Phys. 58 (1985) 2696.
[4] Y. Tsuyoshi, N. Tatsuya, N. Kunihito, Thin Solid Films 381 (2001) 236.
[5] I. Berbezier, J.L. Regolini, C. D'Anterroches, Microsc. Microanal. Microstruct. 4 (1993) 5.
[6] K. Takakura, N. Hiroi, T. Suemasu, S.F. Chichibu, F. Hasegawa, Appl. Phys. Lett. 80 (2002) 556.
[7] A. Terrasi, S. Ravesi, C. Spinella, M.G. Grimaldi, A.L. Mantra, Thin Solid Films 188 (1994) 241.
[8] Z. Yang, K.P. Homewood, M.S. Finney, M.A. Harry, J. Reeson, J. Appl. Phys. 78 (1995) 1958.
[9] Y. Gao, S.P. Wong, Y. Cheung, G. Shao, K.P. Homewood, Nucl. Instr. Meth. B 206 (2003) 317.
[10] M.G. Grimaldi, C. Bongiorno, C. Spinella, E. Grilli, L. Martinelli, M. Gemelli, D.B. Migas, L. Miglio, M. Fanciulli, Phys. Rev. B 66 (2002) 85319.
[11] Y. Maeda, Y. Terai, M. Itakura, N. Kuwano, Thin Solid Films 461 (2004) 160.
[12] S.J. Clark, H.M. Al-Allak, S. Brand, R.A. Abram, Phys. Rev. B 58 (1998) 10389.
[13] D.B. Migas, L. Miglio, Phys. Rev. B 62 (2000) 11063.
[14] Y. Gao, S.P. Wong, W.Y. Cheung, G. Shao, K.P. Homewood, Appl. Phys. Lett. 83 (2003) 42.
[15] G. Shao, K.P. Homewood, Intermetallics 8 (2000) 1405.
[16] T.D. Hunt, K.J. Reeson, K.P. Homewood, S.W. Teon, R.M. Gwilliam, B.J. Sealy, Nucl. Instr. Meth. B 84 (1994) 168.
[17] E.A. Steinmany, H.G. Grimmeiss, Semicond. Sci. Technol. 13 (1998) 124.